New Journal of Physics
The open access journal at the forefront of physics

Deutsche Physikalische Gesellschaft DPG IOP Institute of Physics

PAPER • OPEN ACCESS

Influence of lipid rafts on pattern formation during T-cell adhesion

To cite this article: Long Li *et al* 2021 *New J. Phys.* **23** 043052

New Journal of Physics
The open access journal at the forefront of physics

Deutsche Physikalische Gesellschaft DPG
IOP Institute of Physics

Published in partnership with: Deutsche Physikalische Gesellschaft and the Institute of Physics

OPEN ACCESS

RECEIVED
15 October 2020

REVISED
12 February 2021

ACCEPTED FOR PUBLICATION
1 March 2021

PUBLISHED
4 May 2021

PAPER

Influence of lipid rafts on pattern formation during T-cell adhesion

Long Li[1], Jinglei Hu[2,6,*], Bartosz Różycki[3,*], Xiaohuan Wang[1,4], Helong Wu[5] and Fan Song[1,4]

[1] State Key Laboratory of Nonlinear Mechanics and Beijing Key Laboratory of Engineered Construction and Mechanobiology, Institute of Mechanics, Chinese Academy of Sciences, Beijing 100190, People's Republic of China
[2] Kuang Yaming Honors School & Institute for Brain Sciences, Nanjing University, Nanjing 210023, People's Republic of China
[3] Institute of Physics, Polish Academy of Sciences, Al. Lotników 32/46, Warsaw, Poland
[4] School of Engineering Science, University of Chinese Academy of Sciences, Beijing 100049, People's Republic of China
[5] College of Mechanical Engineering, Zhejiang University of Technology, Hangzhou 310023, People's Republic of China
[6] Shenzhen Research Institute, Nanjing University, Shenzhen 518057, People's Republic of China
[*] Authors to whom any correspondence should be addressed.

E-mail: hujinglei@nju.edu.cn and rozycki@ifpan.edu.pl

Keywords: T-cell adhesion, immunological synapse, pattern formation, lipid raft, intercellular protein binding

Supplementary material for this article is available online

Abstract

Adhesion of T cells to antigen presenting cells is mediated by the TCR–MHCp and LFA1–ICAM1 protein complexes. These intercellular protein complexes segregate and form characteristic special patterns in the cell contact zone. Previous studies have attempted to explain the mechanisms of formation of these patterns. While emphasis has been put on membrane elasticity and active cytoskeletal transport, it remains unclear whether and how the pattern formation process is related to lipid rafts, which are nanoscale molecular clusters enriched in cholesterol and saturated phospholipids in cell membranes. Using Monte Carlo simulations of a statistical mechanical model for T-cell adhesion, we find that lipid rafts can lead to the formation of intermediate pattern with a ring of LFA1–ICAM1 complexes around a central domain of TCR–MHCp complexes even in the absence of active transport of T-cell receptor (TCR) molecules toward the center of the contact zone. In the presence of active TCR transport, lipid rafts can accelerate the formation of this monocentric pattern. We also find that lipid rafts have a strong stabilizing effect on the monocentric pattern after removal of the active TCR transport. Our results not only help to explain recent experimental observations, but also demonstrate that lipid rafts can cooperate with active cytoskeletal transport during the immunological synapse formation.

1. Introduction

T cells can be distinguished from other lymphocytes by the presence of the T-cell receptors (TCRs) in their plasma membrane. They are able to discriminate between healthy and abnormal (e.g. infected or cancerous) cells in the body, based on the peptides presented on the major histocompatibility complexes (MHCs) on the cell surface. The ability of T cells to ignore healthy cells and respond to cells containing pathogenic or cancerous peptides on the MHC molecules is known as antigen discrimination. The molecular mechanisms that underlie this process are controversial.

Adhesion of biological cells is mediated by the formation of intercellular receptor–ligand complexes (figure 1(a)). Important receptor–ligand complexes in the adhesion of T-cells to antigen-presenting cells (APCs) are the TCR–MHCp complex with a length of about 15 nm [1], the CD2–CD48 complex with approximately the same length as TCR–MHCp complex [2–4], and the LFA1–ICAM1 complex with a length of about 40 nm [5]. The difference in lengths between the shorter and longer receptor–ligand complexes leads to a membrane-mediated repulsion between the two types of protein complexes, simply

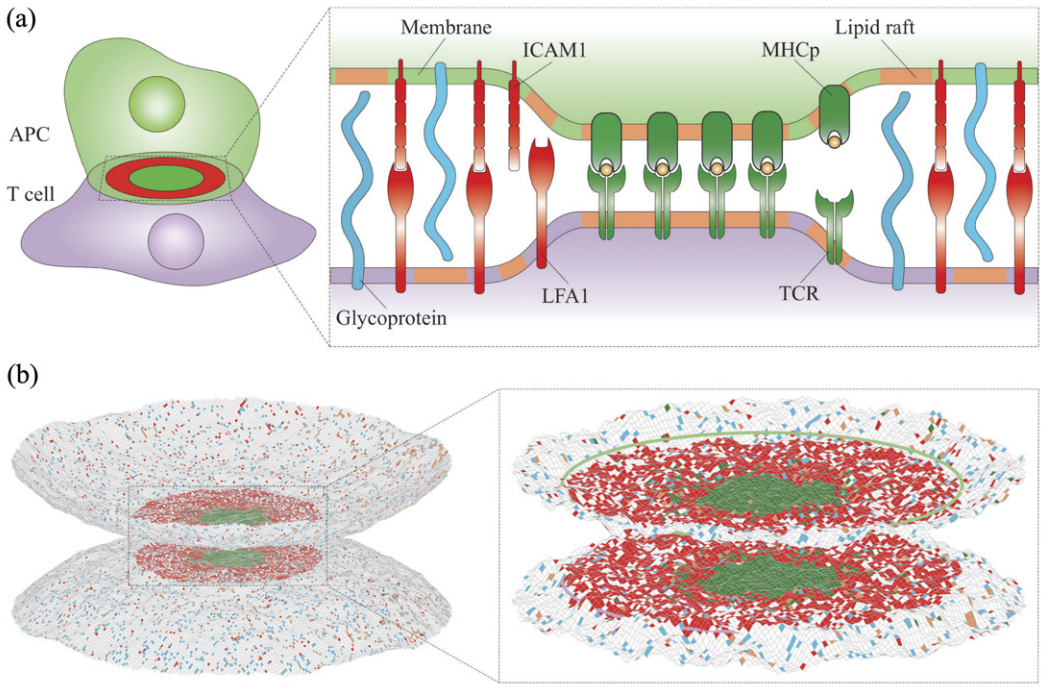

Figure 1. Illustration of the system under study. (a) Cartoon of the intercellular junction between a T cell and an APC known as the immunological synapse with a central domain of TCR–MHCp complexes (green) surrounded by a ring-shaped domain of LFA1–ICAM1 complexes (red). (b) Snapshot from MC simulations of two membranes adhering via specific receptor–ligand binding. Apposing membranes are discretized into square patches with lattice constant $a = 70$ nm. The discretized membranes include a contact zone and a non-adhering zone, which are separated by a border line. Here, the radius of the contact zone is $45a$ and the non-adhering region surrounding the contact zone is a ring of width $55a$. Lipid rafts are colored in orange, TCR and MHCp in green, LFA1 and ICAM1 in red, and glycoprotein in deep sky-blue. A receptor protein binds to a ligand only when they are opposite each other on the two membranes and their distance is within the binding range. Both lipid rafts and proteins diffuse within the membrane surfaces. The different proteins have different affinities for lipid rafts as characterized by coupling energies u_T, u_M, u_L, u_I, u_G given in table 1. An effective attraction between two adjacent raft patches is characterized by contact energy u.

because the lipid membranes have to be bent to compensate for the length mismatch, which costs elastic energy. This membrane-mediated repulsion is additionally increased by the presence of large glycoproteins on the T-cell surface, including CD43 and CD45, which have a length of 40 nm and more [6] and thus form a steric barrier for TCR–MHCp binding. Monte Carlo (MC) simulations and statistical–mechanical calculations have shown that, at physiologically relevant protein concentrations, the membrane-mediated repulsion resulting from the length difference can lead to formation of stable clusters of the receptor–ligand complexes during T-cell adhesion [7, 8]. These clusters can grow into mesoscopic membrane domains, resulting in separation of two phases: one phase enriched in the shorter receptor–ligand complexes, and another phase enriched in the longer receptor–ligand complexes.

Multiple experiments show that the receptor–ligand complexes involved in T-cell adhesion are arranged in characteristic supramolecular patterns: (i) a monocentric pattern consisting of a central domain of TCR–MHCp complexes surrounded by a ring-shaped domain of LFA1–ICAM1 complexes [9–11], (ii) an inverted monocentric pattern consisting of a central domain of LFA1–ICAM1 complexes surrounded by a ring-shaped domain of TCR–MHCp complexes [12–14], or (iii) a multifocal pattern with several nearly circular domains of TCR–MHCp complexes [15, 16]. It is plausible to assume that these domains and patterns can result from the length difference between the TCR–MHCp complexes and other receptor–ligand complexes and proteins in the T-cell adhesion zone [6, 17–22]. However, several other mechanisms have been proposed for the formation of the supramolecular patterns during T-cell adhesion. These mechanisms are based on the active transport by actin cytoskeleton [5, 23], *cis*-interactions between TCRs due to conformational changes induced by ligand binding [24], and pre-clustering of TCRs prior to adhesion [25–27]. These mechanisms certainly do not need to be mutually exclusive. Instead, they may all contribute to the pattern formation and play different roles at different time scales.

Cumulative evidence indicates that cell membranes are structurally and compositionally inhomogeneous at various length scales. In particular, cell membranes contain lipid rafts, which are fluctuating nanoscale molecular clusters enriched in sphingolipid, cholesterol, and proteins [28]. Lipid rafts form platforms that function in membrane signaling and trafficking [28–31]. Interestingly, recent studies show that lipid rafts

may facilitate domain formation during adhesion of cell membranes [32], and provide evidence for the role of lipid rafts in B-cell receptor signaling and a plausible mechanism of B-cell receptor activation via receptor clustering [33]. There is also rich evidence that lipid rafts function in T-cell membranes. First of all, multiple studies have shown that cholesterol levels in the T-cell membrane modulate the TCR clustering and signaling as well as the immunological synapse formation [34–38]. Moreover, lipid rafts have been observed to accumulate in the central zone of the immunological synapse [39] and also to co-localize with anchoring sites of the actin cytoskeleton in the T-cell membrane [5, 40]. Finally, both the TCRs and the MHCp molecules have been reported to have affinity for lipid rafts [41–44]. A natural question thus arises: how do lipid rafts contribute to the pattern formation during T-cell adhesion?

We extend the physical model for T-cell adhesion introduced in reference [45] by incorporating relevant degrees of freedom of lipid rafts (figure 1). Our model takes explicitly into account (i) elastic deformations of the apposing membranes and, thus, the membrane-mediated repulsion between the shorter and longer receptor–ligand complexes, (ii) formation and dissociation of receptor–ligand complexes, (iii) steric repulsion between the apposing membranes due to the presence of glycoproteins in the adhesion zone, (iv) lateral diffusion of membrane proteins, (v) diffusion, fusion and fission of lipid rafts, (vi) interactions of adhesion proteins with lipid rafts, and (vii) active transport of TCR complexes toward the center of the adhesion zone, which is driven by polymerization of the actin cytoskeleton. We study the relative influence of these factors on pattern formation during T-cell adhesion. A major result is that an intermediate monocentric pattern with a central TCR–MHCp domain can be formed without any active transport when the TCR and MHCp molecules have weak affinity for lipid rafts. This monocentric pattern has been observed in earlier computational studies only in the presence of the active radial transport of TCRs [45, 46] because lipid rafts have not been considered in these earlier studies. In the presence of the active TCR transport, lipid rafts can accelerate the formation of the monocentric pattern with the central TCR–MHCp domain surrounded by a ring of LFA1–ICAM1 domain. This finding is consistent with recent experimental observations that increasing the cholesterol level in the T-cell membrane causes enhanced TCR clustering and more efficient formation of the mature immunological synapse [37]. We quantify the impact of lipid rafts on different dynamic regimes during T-cell adhesion as well as on the kinetics of domain formation.

2. Model

As illustrated in figure 1(a), the T-cell membrane contains the TCR and LFA1 molecules (receptors), whereas the APC membrane contains the MHCp and ICAM1 molecules (ligands). Both membranes contain glycoproteins and lipid rafts. As illustrated in figure 1(b), the membranes are represented by two-dimensional lattices. Each of the two membranes is divided into a circular contact zone and a surrounding region in which the membranes do not interact. The receptors diffuse in the whole T-cell membrane, but interact with the ligands diffusing in the APC membrane only within the contact zone of the two membranes. The non-adhering regions can be thus regarded as reservoirs of the membrane proteins.

As in reference [45], the lattice spacing is taken to be $a = 70$ nm and the radius of the circular contact zone is $45a$. The distance between the two membranes at the rim of the contact zone is fixed at a value of 100 nm, which is significantly larger than the length of the TCR–MHCp and LFA1–ICAM1 complexes and of the glycoproteins. In each of the two membranes, the non-adhering segment surrounding the contact zone is a ring of width $55a$.

The energy of elastic deformations of the two membranes is given by a discrete representation of the Helfrich Hamiltonian

$$\mathcal{H}_{\rm el} = \sum_i \left[\frac{\kappa}{2a^2}(\Delta_{\rm d} l_i)^2 + \frac{\sigma}{2}(\nabla_{\rm d} l_i)^2\right], \tag{1}$$

where $\kappa = \kappa_{\rm T}\kappa_{\rm A}/(\kappa_{\rm T} + \kappa_{\rm A})$ is an effective bending rigidity of the two membranes with rigidity moduli $\kappa_{\rm T}$ and $\kappa_{\rm A}$; $\sigma = (\sigma_{\rm T}\kappa_{\rm T}^2 + \sigma_{\rm A}\kappa_{\rm A}^2)/(\kappa_{\rm T} + \kappa_{\rm A})^2$ is an effective surface tension for the membranes subject to tensions $\sigma_{\rm T}$ and $\sigma_{\rm A}$; l_i is the local separation between the two membranes at lattice site i; whereas $\nabla_{\rm d} l_i/a$ and $\Delta_{\rm d} l_i/a^2$, respectively, are the discretized gradient and Laplacian of the separation field $\{l_i\}$. The bending rigidities of the T-cell and APC membranes take the typical value of $\kappa_{\rm T} = \kappa_{\rm A} = 25 k_{\rm B}T$, leading to $\kappa = 12.5 k_{\rm B}T$ [47], where $k_{\rm B}$ and T denote the Boltzmann constant and temperature, respectively. For the effective tension, we choose the value $\sigma = 0.1\kappa/a^2$ as in references [45–49].

Each site at the membrane lattices can accommodate multiple proteins. The spatial distribution of receptors in the T-cell membrane is described by three sets of non-negative integer variables: $\{m_i^{\rm T}\}$ for TCRs, $\{m_i^{\rm L}\}$ for LFA1 molecules, and $\{m_i^{\rm GT}\}$ for glycoproteins, where subscript i labels the lattice sites.

Table 1. Parameters used in MC simulations.

Parameter	Definition	Value	References
a	Lattice spacing	70 nm	[45, 48]
r_1	Radius of the circular contact zone	$45a$	[45, 48]
r_2	Radius of the circular simulation domain	$100a$	[45, 48]
D	Protein diffusion constant	1 $\mu m^2\ s^{-1}$	[65, 66]
κ_T	Bending rigidity of T-cell membrane	$25k_BT$	[47]
κ_A	Bending rigidity of APC membrane	$25k_BT$	[47]
κ	Effective bending rigidity	$12.5k_BT$	[47]
σ	Lateral tension	$0.1\kappa/a^2$	[45, 48, 49]
c_T	Area concentration of TCR molecules	100/μm^2	[19]
c_M	Area concentration of MHCp molecules	75/μm^2	[12, 19]
c_L	Area concentration of LFA1 molecules	100/μm^2	[19]
c_I	Area concentration of ICAM1 molecules	100/μm^2	[12, 19]
c_G	Area concentration of glycoproteins	50/μm^2	[45]
l_{TM}	Length of the TCR–MHCp complex	15 nm	[50, 51]
l_{LI}	Length of the LFA1–ICAM1 complex	40 nm	[50, 51]
l_G	Length of glycoproteins	40 nm	[50, 51]
l_B	Receptor-ligand binding range	10 nm	[45]
u_{TM}	Binding energy of TCR and MHCp	$2–8k_BT$	[45]
u_{LI}	Binding energy of LFA1 and ICAM1	$2–8k_BT$	[45]
w_G	Repulsive strength imposed by glycoproteins	$10\kappa/a^2$	[45]
u_T	Affinity of TCR for lipid rafts	$-3–0k_BT$	[58]
u_M	Affinity of MHCp for lipid rafts	$-3–0k_BT$	[44]
u_L	Affinity of LFA1 for lipid rafts	$-1–3k_BT$	[59, 60]
u_I	Affinity of ICAM1 for lipid rafts	$-1–3k_BT$	[44, 61]
u_G	Affinity of glycoprotein for lipid rafts	$1k_BT$	[55, 62]
u^*	Critical contact energy in 2D lattice gas model	$2\ \ln(1+\sqrt{2})k_BT$	[32]
u	Energy of contact between lipid rafts	$0.7–0.9u^*$	[32]
x	Area fraction of lipid rafts	0–0.3	[55–57]
f	Force pulling TCR molecules	$0.01–0.1k_BT/a$	[45]

Likewise, the distribution of ligands in the APC membrane is given by $\{m_i^M\}$ for MHCp molecules, $\{m_i^I\}$ for ICAM1 proteins, and $\{m_i^{GA}\}$ for glycoproteins. The interactions between the receptors and ligands are captured by square-well potentials that together give rise to the adhesion energy

$$\mathcal{H}_{ad} = -\sum_i \left[\min(m_i^T, m_i^M) u_{TM}\theta\left(\frac{1}{2}l_b - |l_i - l_{TM}|\right) + \min(m_i^L, m_i^I) u_{LI}\theta\left(\frac{1}{2}l_b - |l_i - l_{LI}|\right)\right]. \quad (2)$$

Here, l_{TM} and l_{LI} are the lengths of the TCR–MHCp and LFA1–ICAM1 complexes, respectively; l_b is the width of the square-well potentials; and u_{TM} and u_{LI} are the potential depths for TCR–MHCp and LFA1–ICAM1, respectively. The Heaviside's function $\theta(\cdots)$ ensures the specificity of the receptor–ligand binding. We take $l_{TM} = 15$ nm, $l_{LI} = 40$ nm, and $l_b = 10$ nm [45, 50, 51]. The energy of the receptor–ligand binding, u_{TM} and u_{LI}, are in the range between 2 and $8k_BT$ [45].

The steric repulsion imposed by glycoproteins embedded in both membranes is modeled by truncated harmonic potentials

$$\mathcal{H}_{st} = \sum_i \left(m_i^{GT} + m_i^{GA}\right) w_G (l_G - l_i)^2 \theta\left(l_G - l_i\right) \quad (3)$$

with the repulsion strength $w_G = 10\kappa/a^2$ and the length of glycoproteins $l_G = 40$ nm [45, 50, 51]. The area concentrations of the membrane proteins are taken in accord to literature data [12, 19, 45, 48, 50, 52–54], as summarized in table 1.

The spatial distributions of lipid rafts in the T-cell and APC membranes are described by sets of composition variables $\{n_i^T\}$ and $\{n_i^A\}$, respectively. Each of these variables takes values 0 or 1 indicating, respectively, the absence or presence of a lipid raft at site i. Since lipid rafts have a propensity to coalesce due to their hydrophobic mismatch with the membrane matrix, we introduce an energy term which describes attraction between lipid rafts at nearest-neighbor membrane sites and which is analogous to the Hamiltonian of the two-dimensional lattice-gas model

$$\mathcal{H}_{at} = -u\sum_{\langle i,j\rangle}\left(n_i^T n_j^T + n_i^A n_j^A\right). \quad (4)$$

Here, u is the contact energy and the sum runs over all pairs of nearest-neighbor sites in each of the two membranes. To investigate how the energy of boundaries between the membrane matrix and lipid rafts affects pattern formation during T-cell adhesion, we vary u in the range between $0.7u^*$ and $0.9u^*$, where

$u^* = 2\ln(1+\sqrt{2})k_BT$ is the contact energy at the critical point of the two-dimensional lattice-gas model. With this choice of u-values, lipid rafts do not coalesce into stable mesoscopic domains in free, non-adhering membranes.

It is useful to define the fractions of lattice sites containing lipid rafts in the T-cell membrane $x_T = \frac{1}{N}\sum_i n_i^T$ and in the APC membrane $x_A = \frac{1}{N}\sum_i n_i^T$ where N is the total number of sites in each of the membranes. Without loss of generality, and to reduce the number of model parameters, we assume a symmetry in the lipid composition of the two membranes and, thus, take $x \equiv x_T = x_A$ as a relevant parameter. Based on variations in the amount of raft-favoring lipids that have been reported to accompany intercellular interaction process [55], we vary x up to the value of 0.3 [55–57].

Experimental studies suggest that the TCR and MHCp molecules have affinity for lipid rafts [44, 58], whereas different experiments lead to ambiguous conclusions on whether the LFA1 and ICAM1 proteins have a propensity to co-localize with lipid rafts or not [44, 59–61]. Glycoproteins exhibit different affinities for lipid rafts, e.g. CD45 has been reported to be excluded from rafts [55], in contrast to CD43 which co-localizes with rafts [62]. To take into account the different affinities of the receptor and ligand proteins for lipid rafts, we introduce an extra term for the energy of protein-raft coupling

$$\mathcal{H}_{co} = \sum_i \left[u_T m_i^T n_i^T + u_M m_i^M n_i^A + u_L m_i^L n_i^T + u_I m_i^I n_i^A + u_G (m_i^{GT} n_i^T + m_i^{GA} n_i^A)\right]. \tag{5}$$

The values of coupling energies u_T, u_M, u_L, u_I and u_G are listed in table 1. The negative values indicate that the proteins have a propensity to associate with lipid rafts. The positive values mean that the proteins are effectively excluded from lipid rafts.

Polymerization of the actin cytoskeleton during T-cell adhesion drives an active transport of TCRs toward the center of the contact zone [63]. As in reference [45], this active transport is simulated here as directed diffusion of TCRs, i.e., a constant force f acts on each of the TCR molecules in the direction of the center of the contact zone. The action of this force introduces an additional energy term

$$\mathcal{H}_{ac} = \sum_i f r_i^T m_i^T, \tag{6}$$

where r_i^T denotes the distance of the TCRs at site i from the center of the contact zone.

We employ the MC method with the standard Metropolis criterion to simulate the membrane system defined by Hamiltonian $\mathcal{H} = \mathcal{H}_{el} + \mathcal{H}_{ad} + \mathcal{H}_{st} + \mathcal{H}_{at} + \mathcal{H}_{co} + \mathcal{H}_{ac}$, which comprises the energy terms given by equations (1)–(6). The MC simulations comprise three types of trial moves: (i) variations in the local separation between the two membranes, l_i, which capture vertical displacements of the membranes due to thermal fluctuations, (ii) lateral translations of the receptor and ligand molecules as well as glycoproteins, which represent their diffusion, and (iii) lateral translations of lipid rafts. The trial moves (ii) and (iii) are realized by random jumps to one of the four nearest-neighbor sites. In trial moves (iii), the proteins within the raft sites are not attempted to move along with the rafts. The proportion of the moves (i), (ii) and (iii) in each of the MC sweeps is chosen according to the physical timescales as in reference [64]. The values of parameters used in the MC simulations are chosen according to experimental results and existing literature data (see table 1). Assuming the typical diffusion coefficient $D = 1\ \mu m^2\ s^{-1}$ for membrane proteins, the diffusion time for a free protein moving a distance $a = 70$ nm to a neighboring membrane patch in a single MC sweep is $t = a^2/(4D) \approx 1$ ms. Thus, a single MC sweep roughly corresponds to the physical time of 1 ms.

In our simulations, the overall numbers of raft sites and each type of proteins are all kept fixed in the whole system, whereas the corresponding numbers in the contact zone vary during adhesion. We observe that there are raft sites and proteins remaining in the non-adhering region of the membranes even when the final patterns are formed. The pattern formation process therefore is not biased by constraints of fixed concentrations of rafts or proteins in the contact zone. As stated in reference [45], the choice of the adhesion geometry shown in figure 1(b) makes it possible to avoid the difficulty of modeling the complete shape of the cell. It is assumed that the contact zone has a circular shape and constant area on the time scales considered here. We set initial membrane separations $l_i = l_0 + cr_i^4$ with $l_0 = 45$ nm larger than the lengths of both glycoproteins and the two types of receptor–ligand complexes so that the proteins and complexes can freely diffuse into and out of the region before cell contact. Here, r_i is the lateral distance from site i to the center of the contact zone (figure 1(b)), and the parameter c is chosen to attain a membrane separation $l_{rim} = 100$ nm at the rim of the contact zone unless otherwise specified. The reflecting boundary conditions are imposed at the outer rim of the non-adhering region.

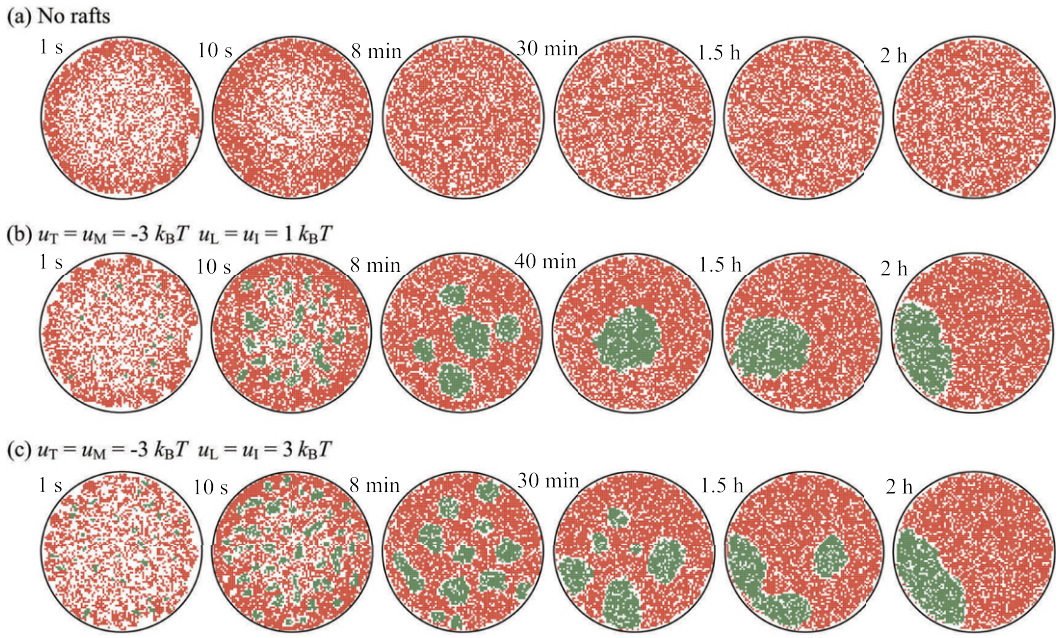

Figure 2. Three sequences of typical adhesion patterns (top views on the cell contact zone). Membrane sites with the TCR–MHCp and LFA1–ICAM1 complexes are shown in green and red, respectively. The black circle represents the boundary of the contact zone. The receptor–ligand binding energies are $u_{TM} = 2k_BT$ for the TCR–MHCp complex and $u_{LI} = 8k_BT$ for LFA1–ICAM1 complex. The TCR–MHCp complexes are not observed in the absence of lipid rafts (a). However, in the presence of lipid rafts, either the intermediate monocentric pattern (b) or the intermediate multifocal patterns (c) are observed, depending on the strength of repulsion of the LFA1 and ICAM1 proteins from lipid rafts, which are quantified here by coupling energies $u_L = u_I = 1k_BT$ in (b) and $u_L = u_I = 3k_BT$ in (c). In both (b) and (c), the affinity of the TCR and MHCp molecules for lipid rafts is described by coupling energies $u_T = u_M = -3k_BT$. The interactions of glycoproteins with lipid rafts are weakly repulsive and quantified by $u_G = 1k_BT$. The effective attraction between lipid rafts is described by contact energy $u = 0.8u^*$, where $u^* = 2\ \ln(1+\sqrt{2})k_BT$ is the critical contact energy for the two-dimensional lattice-gas model. The area fraction of lipid rafts is $x = 0.3$.

3. Results and discussion

To study the influence of lipid rafts on pattern formation during T-cell adhesion, we performed MC simulations with different values of parameters characterizing the molecular interactions within the immunological synapse. Figure 2 shows typical sequences of patterns (top views on the cell contact zone) obtained from MC simulations with the binding energy of TCR–MHCp ($u_{TM} = 2k_BT$) smaller than that of LFA1–ICAM1 ($u_{LI} = 8k_BT$). Membrane sites with the intercellular TCR–MHCp and LFA1–ICAM1 complexes are shown in green and red, respectively. The sequences of pattern formation shown in figure 2 (as well as other figures) are taken from 5–10 independent simulation runs for each adhesion system with different initial distributions of the proteins and lipid rafts. Each of the 5–10 runs leads to similar sequences of patterns (see, for instance, figures 2(b) and S1 (https://stacks.iop.org/NJP/23/043052/mmedia)).

In the absence of lipid rafts (figure 2(a)), the TCR–MHCp complexes are not observed in the contact zone and the two membranes adhere only via the LFA1–ICAM1 complexes. The reason for the absence of the TCR–MHCp complexes in the contact zone is that the weak TCR–MHCp binding cannot compensate the energy cost of membrane bending imposed by the length mismatch between the short TCR–MHCp complexes and the long LFA1–ICAM1 complexes. In the presence of lipid rafts (figures 2(b) and (c)), however, mesoscopic domains of the TCR–MHCp complexes are observed in the contact zone. The formation of these domains is caused not only by the length difference between the TCR–MHCp and LFA1–ICAM1 complexes [7, 8], but also by three other factors, namely, (i) the affinity of the TCR and MHCp molecules for lipid rafts, which is described here by coupling energies $u_T = u_M = -3k_BT$, (ii) the propensity of lipid rafts to coalesce due to their hydrophobic mismatch with the membrane matrix, which is captured in the MC simulations by contact energy u (see section 2 for details), and (iii) the relatively weak attraction or even repulsion of the LFA1 and ICAM1 proteins with lipid rafts, as quantified here by coupling energies $u_L = u_I > -3k_BT$ (see also figure S2). Here, the contact energy is relatively small so that lipid rafts do not coalesce into large-scale domains in free, non-adhering membranes. Specifically, $u = 0.8u^* \approx 1.4k_BT$. In order to investigate how raft aggregation affects the pattern formation, we also consider other values of u, as shown in figure 6.

The interactions of the membrane proteins with lipid rafts affect the energetics of receptor–ligand binding and, thus, also the dynamics of pattern formation during T-cell adhesion. Figure 2 shows that, in the presence of lipid rafts in the membranes, many separate domains of the TCR–MHCp complexes are formed within the first several minutes after cell membrane contact, implying that lipid rafts enhance the binding and clustering of TCR–MHCp. To distinguish the pattern formation at different conditions, we identify the intermediate patterns according to the algorithm described in the supplementary material. If the LFA1 and ICAM1 molecules exhibit weaker attraction (figure S2(a), $u_{\rm L} = u_{\rm I} = -1k_{\rm B}T$) or gentle repulsion (figure 2(b), $u_{\rm L} = u_{\rm I} = 1k_{\rm B}T$) from lipid rafts, these early TCR–MHCp domains prefer to grow and coalesce in the interior of the contact zone and form the intermediate monocentric pattern, which persists for nearly 1 h and eventually transforms into a final, lens-shape domain at the periphery of the contact zone. To confirm that the transient monocentric pattern is not an artifact caused by the boundary conditions with a fixed membrane separation $l_{\rm rim}$ at the rim of the contact zone, we performed additional simulations with different values of $l_{\rm rim}$ and observed analogous sequences of pattern formation as shown in figure S3. In contrast to the scenario in figure 2(b), if the effective repulsion of the LFA1 and ICAM1 molecules from lipid rafts is somewhat stronger (figure 2(c), $u_{\rm L} = u_{\rm I} = 3k_{\rm B}T$), the early TCR–MHCp domains coalesce and grow in the whole contact zone, but do not transform into the intermediate monocentric pattern; instead, one observes the intermediate multifocal patterns, which eventually transform into the final, lens-shape domain aside the contact zone. Therefore, stronger exclusion of the LFA1 and ICAM1 molecules from lipid rafts not only extends the lifetime of the early TCR–MHCp domains but also facilitates the formation of the intermediate multifocal patterns. The occurrence of intermediate multifocal patterns reflects the fact that the TCR–MHCp binding is further enhanced by the strong exclusion of the LFA1 and ICAM1 molecules from lipid rafts and can well compensate the energy cost of membrane bending required for the formation of TCR–MHCp complexes at the periphery. Such enhancement is also evidenced by the appearance of more separate TCR–MHCp domains at $t = 1$ s compared to those shown in figure 2(b). Control simulations with other sets of coupling energies between lipid rafts and adhesion proteins reveal that the exclusion of LFA1 and ICAM1 from lipid rafts alone (figures S2(b) and S2(c), $u_{\rm T} = u_{\rm M} = 0$, $u_{\rm L} = u_{\rm I} > 0$) is not sufficient for the formation of intermediate monocentric patterns, and that the equal affinities of adhesion proteins for lipid rafts (figure S2(d), $u_{\rm T} = u_{\rm M} = -1k_{\rm B}T$, $u_{\rm L} = u_{\rm I} = -1k_{\rm B}T$) do not lead to the formation of TCR–MHCp domains.

The adhesion patterns shown in figure 2 represent a scenario in which the binding of LFA1 and ICAM1 is stronger than the binding of TCR and MHCp. It is interesting and important, however, to explore how the pattern formation depends on the strength of receptor–ligand binding. As a matter of fact, the TCR–MHCp binding strength is an important control parameter as it depends on the peptide displayed on the MHC molecules, which must be recognized by the T cell. Figure 3 shows three sequences of adhesion patterns that come from MC simulations with the binding energy of TCR–MHCp ($u_{\rm TM} = 4k_{\rm B}T$) comparable to that of LFA1–ICAM1 ($u_{\rm LI} = 3k_{\rm B}T$). The intermediate patterns shown in figure 3 are indeed qualitatively different than those displayed in figure 2. In the absence of lipid rafts in the membranes (figure 3(a)), one observes the intermediate multifocal patterns that evolve directly into the final, lens-shape domain. In the presence of lipid rafts in the membranes (figures 3(b) and (c)), in contrast, one observes the intermediate inverted monocentric pattern, which persists for about 1 h and transforms into the final, lens-shape domain aside the contact zone. The intermediate inverted monocentric pattern is formed earlier and lasts longer as the repulsion of the LFA1 and ICAM1 molecules from lipid rafts is increased from $u_{\rm L} = u_{\rm I} = 1k_{\rm B}T$ (figure 3(b)) to $u_{\rm L} = u_{\rm I} = 3k_{\rm B}T$ (figure 3(c)). The formation of the peripheral ring of the TCR–MHCp complexes (figures 3(b) and (c)) is controlled by diffusion of the TCR and MHCp molecules into the contact zone. If it were not so, one would observe either the growth of large domains at the cost of small ones, or domain coalescence, but neither would occur necessarily at the periphery of the contact zone. Therefore, the TCR–MHCp complex formation does not require crossing of free-energy barriers, which is consistent with the observation that the TCR–MHCp binding is effectively enhanced in the presence of lipid rafts.

Figure 4 shows three sequences of adhesion patterns obtained from MC simulations with the binding energy of TCR–MHCp ($u_{\rm TM} = 6k_{\rm B}T$) larger than that of LFA1–ICAM1 ($u_{\rm LI} = 2k_{\rm B}T$). In this case, the presence of lipid rafts does not change the characteristics of pattern evolution. Namely, many small domains of the TCR–MHCp complexes initially nucleate in the contact zone, then they form the intermediate inverted monocentric pattern, which eventually transforms into the lens-shape domain at the periphery of the contact zone. The sequences of patterns shown in figure 4 are expectedly quite similar to those in figures 3(b) and (c), because the TCR–MHCp binding is in these cases strong enough to overcome the energy of membrane deformations required by the length difference between the TCR–MHCp and

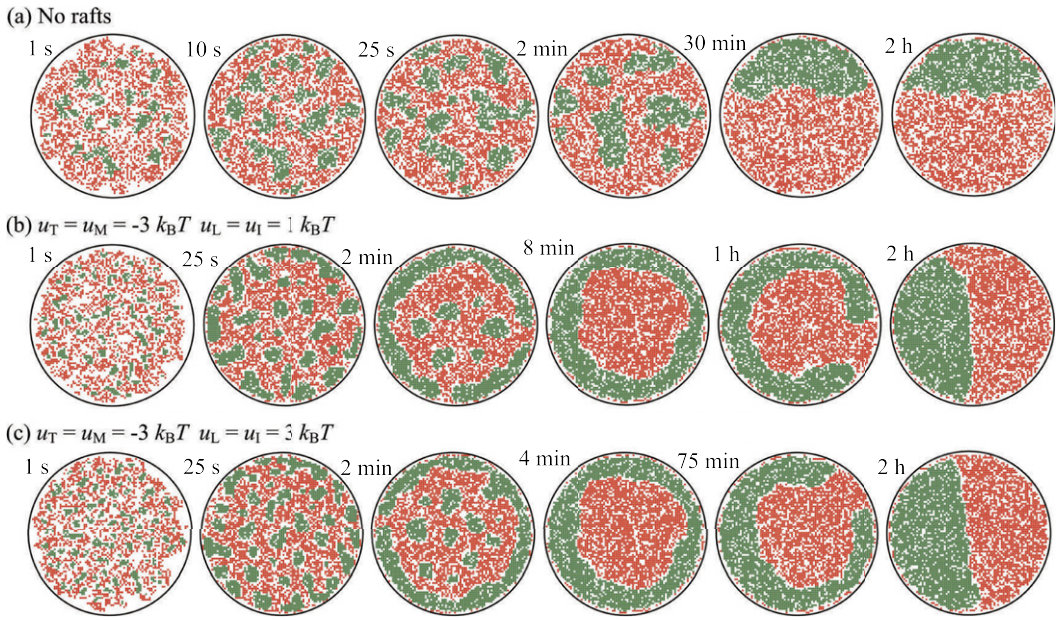

Figure 3. Analogous to figure 2 but for binding energies $u_{TM} = 4k_BT$ and $u_{LI} = 3k_BT$. The intermediate pattern is multifocal in (a) and inverted monocentric in (b) and (c). The inverted monocentric pattern is formed earlier and lasts longer as the repulsion of LFA1 and ICAM1 from lipid rafts is increased.

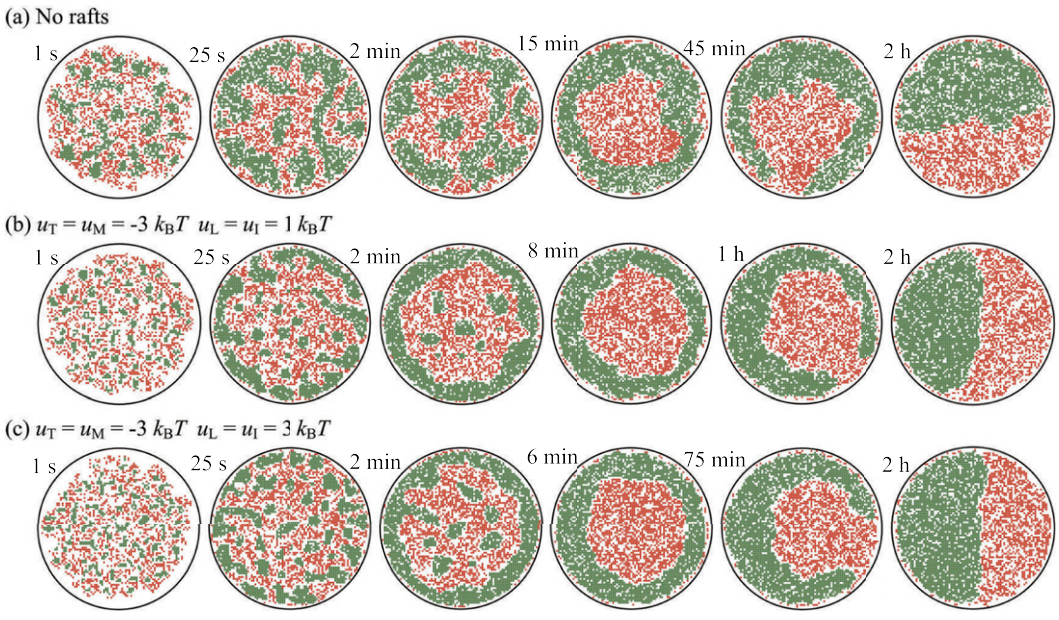

Figure 4. Analogous to figure 3 but for binding energies $u_{TM} = 6k_BT$ and $u_{LI} = 2k_BT$. The inverted monocentric pattern remains unchanged by lipid rafts. However, this pattern is formed earlier and lasts longer with the increase of repulsion of LFA1 and ICAM1 from lipid rafts.

LFA1–ICAM1 complexes, and then diffusion of the TCR and MHCp molecules into the contact zone leads to the formation of the TCR–MHCp ring.

A comparison of figures 2–4 shows that the pattern evolution depends critically on the presence or absence of lipid rafts in the membranes as well as on the receptor–ligand binding energies u_{TM} and u_{LI}. We thus performed extensive MC simulations with different values of parameters u_{TM} and u_{LI} ranging from 2 to $8k_BT$ and used the algorithm described in the supplementary material to identify the intermediate patterns. Figure 5 summarizes the intermediate patterns observed in the MC simulations. For membranes without lipid rafts (figure 5(a)), the diagram of intermediate patterns is fully consistent with the results reported by Weikl and Lipowsky [45]. Namely, for rather weak TCR–MHCp binding, the membrane adhesion is mediated only by the LFA1–ICAM1 complexes and the TCR–MHCp complexes are not

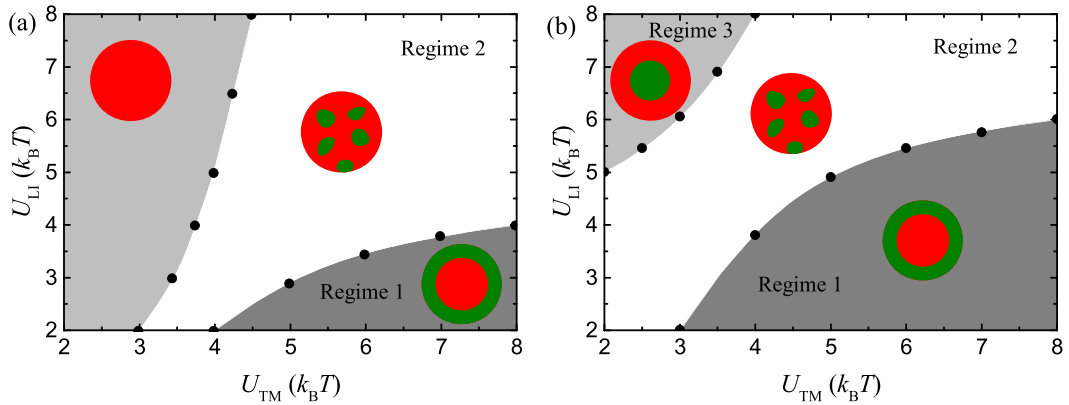

Figure 5. Dynamic regimes for T-cell adhesion in the absence (a) and presence (b) of lipid rafts. In panel (b), $u_T = u_M = -3k_BT$, $u_L = u_I = 1k_BT$, $u_G = 1k_BT$, $u = 0.8u^*$ and $x = 0.3$, as in figure 2(b). The filled circles represent data points obtained from the MC simulations.

observed in the contact zone. For sufficiently strong TCR–MHCp binding, one can distinguish two dynamic regimes, i.e., regime 1 with the intermediate inverted monocentric pattern for relatively weak LFA1–ICAM1 binding, and regime 2 with the intermediate multifocal pattern for comparable strengths of the TCR–MHCp and LFA1–ICAM1 binding. For membranes containing lipid rafts (figure 5(b)), in contrast, one additionally observes regime 3 with the intermediate monocentric pattern for weak TCR–MHCp binding and sufficiently strong LFA1–ICAM1 binding. The boundaries between these regimes depend on the values of model parameters. The data shown in figure 5(b) come from MC simulations with $u_T = u_M = -3k_BT$, $u_L = u_I = 1k_BT$, $u_G = 1k_BT$, $u = 0.8u^*$ and $x = 0.3$. It is important to note that regime 3 with the monocentric pattern is never observed in the adhering membranes without lipid rafts, unless active transport of TCRs to the center of the contact zone is taken into account [45].

In addition to the adhesion proteins with specific binding interactions, the cell membranes contain glycoproteins such as CD43 and CD45. These glycoproteins have similar lengths as the LFA1–ICAM1 complexes and therefore can enter the LFA1–ICAM1 domains, but are excluded from the TCR–MHCp domains in the contact zone. Making the area concentration of the glycoproteins larger thus has a similar effect as increasing the binding energy U_{LI} of the LFA1–ICAM1 complexes, as shown in figure 5 in reference [45]. Since in this study we are mainly focused on the effect of lipid rafts on the adhesion dynamics, in our simulations we fix the area concentration of glycoproteins at the level of $50/\mu m^2$ in each of the apposing membranes.

Another relevant control parameter, in addition to the binding energies u_{TM} and u_{LI}, is the contact energy, u, which quantifies the energy of boundaries between the membrane matrix and lipid rafts. Figure 6 shows sequences of adhesion patterns obtained from MC simulations with different values of u and binding energies $u_{TM} = 2k_BT$ and $u_{LI} = 8k_BT$. For $u = 0.7u^*$ (figure 6(a)) and $u = 0.8u^*$ (figure 6(b)), the intermediate monocentric pattern persists for up to 1 h. Such a pattern is formed earlier and lasts longer for $u = 0.8u^*$ than for $u = 0.7u^*$. But for $u = 0.9u^*$ (figure 6(c)), when lipid rafts have a stronger propensity to coalesce, the intermediate monocentric pattern does not form. Instead, the multifocal patterns transform directly into the final, lens-shaped domain aside the contact zone.

The contact energy can also facilitate formation of the inverted monocentric pattern. Figure 7 shows sequences of adhesion patterns obtained from MC simulations with the binding energies $u_{TM} = 4k_BT$ and $u_{LI} = 3k_BT$ and with different values of u. The values of other parameters are the same as in figure 6. For $u = 0.7u^*$ (figure 7(a)), initial domains of the TCR–MHCp complexes grow but do not form a complete intermediate ring-shaped domain. For $u = 0.8u^*$ (figure 7(b)) and $u = 0.9u^*$ (figure 7(c)), however, initial patterns transform into the intermediate inverted monocentric pattern, which is formed earlier and lasts longer with increasing values of u.

Another parameter that affects the type of intermediate patterns is the area fraction x of lipid rafts in the membranes. Figure 8 shows typical sequences of patterns obtained from MC simulations with different values of x. Here, the binding energies are $u_{TM} = 3k_BT$ and $u_{LI} = 2k_BT$. The contact energy $u = 0.8u^*$ and the interactions of the membrane proteins with lipid rafts are described by coupling energies $u_T = u_M = -3k_BT$, $u_L = u_I = 1k_BT$ and $u_G = 1k_BT$. For $x = 0$ (figure 8(a)), i.e. in the absence of lipid rafts, membrane domains containing the TCR–MHCp complexes can hardly be formed in the contact zone. For $x = 0.05$ (figure 8(b)), the intermediate monocentric pattern is observed. For $x = 0.1$ (figure 8(c)), the

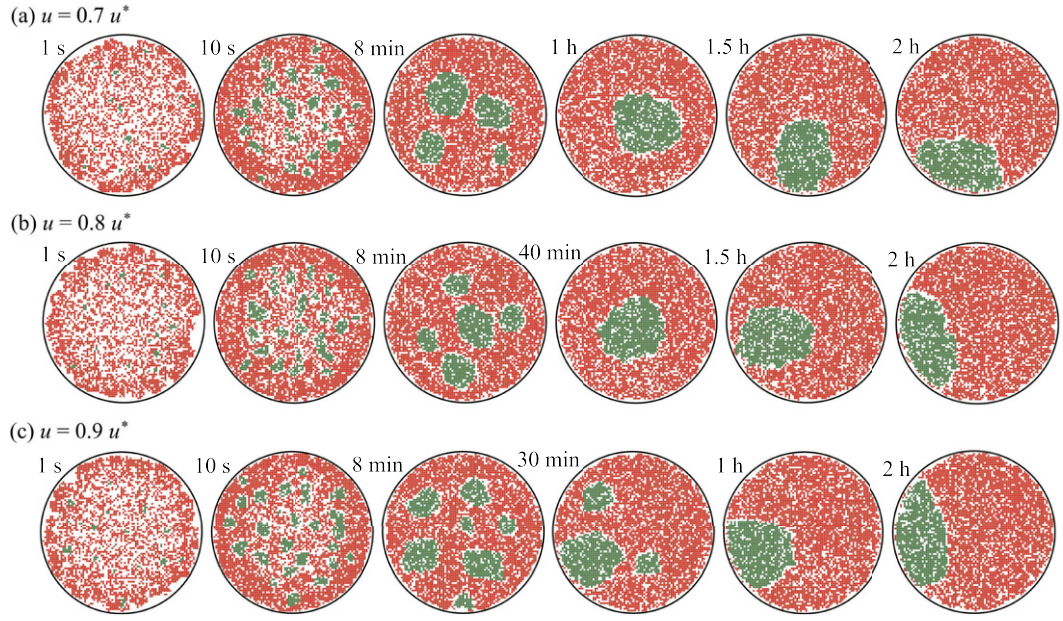

Figure 6. Three sequences of typical pattern evolution obtained from MC simulations with different values of contact energy, u, as indicated in each of the panels. The binding energies are $u_{TM} = 2k_BT$ and $u_{LI} = 8k_BT$. The intermediate monocentric pattern remains unchanged if u is increased from $0.7u^*$ (a) to $0.8u^*$ (b), but this pattern is formed earlier and lasts longer for larger values of u (b). However, if u is increased up to $u = 0.9u^*$ (c), the intermediate monocentric pattern is replaced by the intermediate multifocal pattern. The values of other parameters are as follows: $u_T = u_M = -3k_BT$, $u_L = u_I = 1k_BT$, $u_G = 1k_BT$ and $x = 0.3$.

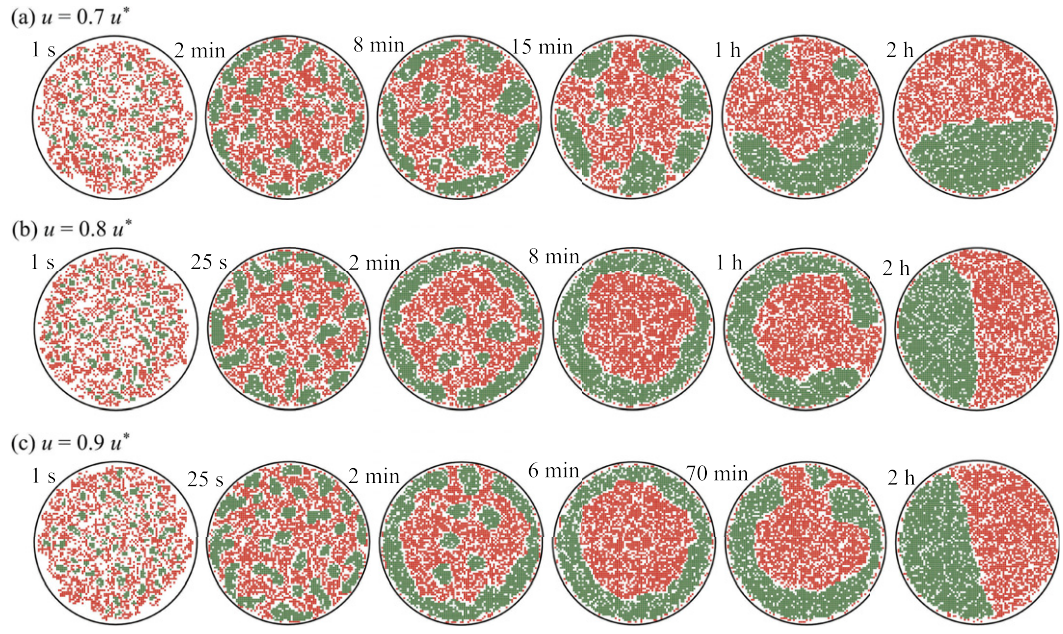

Figure 7. Analogous to figure 6 but for binding energies $u_{TM} = 4k_BT$ and $u_{LI} = 3k_BT$. Here, increasing the effective attraction between lipid rafts, u, results in the formation of the inverted monocentric pattern (b, c). This pattern is formed earlier and lasts longer with increasing values of u.

intermediate multifocal pattern is observed. Finally, for $x = 0.3$ (figure 8(d)), an intermediate pattern is the inverted monocentric pattern.

The results presented in figures 2–8 were obtained from MC simulations without the active transport of TCRs toward the center of the contact zone, i.e. with $f = 0$ in equation (6). In order to investigate how lipid rafts can cooperate with the actin cytoskeleton in the processes of immunological synapse formation, we also performed MC simulations with $f > 0$. Figure 9 shows two sequences of adhesion patterns obtained from MC simulations with the binding energies $u_{TM} = 2k_BT$ and $u_{LI} = 8k_BT$ and the constant force $f = 0.01k_BT/a$. One pattern sequence (figure 9(a)) was obtained from MC simulations of membranes

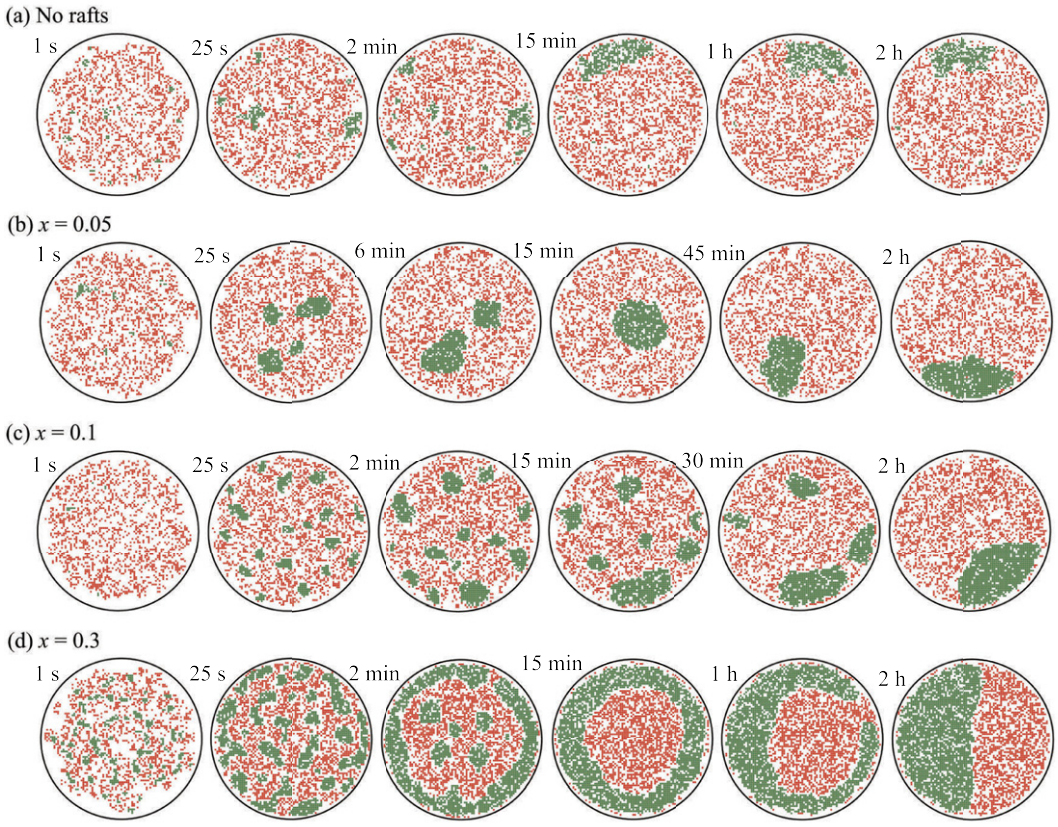

Figure 8. Four sequences of typical pattern evolution obtained from MC simulations with different area fractions of lipid rafts, x, as indicated in each of the panels. At $t = 15$ min, the monocentric pattern, multifocal pattern, and inverted pattern are observed for x equal to 0.05, 0.1 and 0.3, respectively. The values of model parameters are as follows: $u_{\mathrm{TM}} = 3k_{\mathrm{B}}T$, $u_{\mathrm{LI}} = 2k_{\mathrm{B}}T$, $u_{\mathrm{T}} = u_{\mathrm{M}} = -3k_{\mathrm{B}}T$, $u_{\mathrm{L}} = u_{\mathrm{I}} = 1k_{\mathrm{B}}T$, $u_{\mathrm{G}} = 1k_{\mathrm{B}}T$ and $u = 0.8u^{*}$.

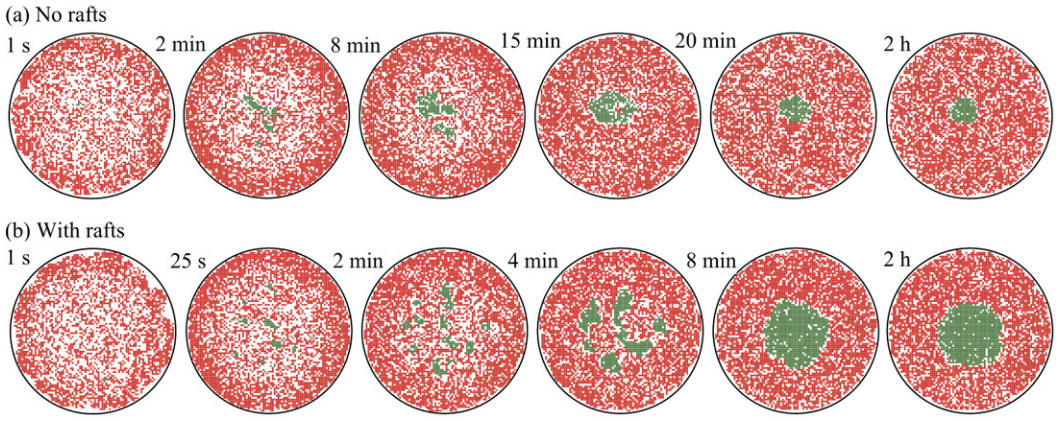

Figure 9. Typical pattern evolution with active transport of TCRs to the center of the contact zone. Panels (a) and (b) correspond to the absence and presence of lipid rafts, respectively. In the MC simulations, force $f = 0.01k_{\mathrm{B}}T/a$ acts concentrically on TCRs. In both (a) and (b), the binding energies are $u_{\mathrm{TM}} = 2k_{\mathrm{B}}T$ and $u_{\mathrm{LI}} = 8k_{\mathrm{B}}T$. The values of other parameters in (b) are as follows: $u_{\mathrm{T}} = u_{\mathrm{M}} = -3k_{\mathrm{B}}T$, $u_{\mathrm{L}} = u_{\mathrm{I}} = 1k_{\mathrm{B}}T$, $u_{\mathrm{G}} = 1k_{\mathrm{B}}T$, $u = 0.8u^{*}$ and $x = 0.3$.

without lipid rafts. The other sequence of patterns (figure 9(b)) was obtained from MC simulations with the fraction of raft patches of $x = 0.3$; the values of other parameters were set to $u_{\mathrm{T}} = u_{\mathrm{M}} = -3k_{\mathrm{B}}T$, $u_{\mathrm{L}} = u_{\mathrm{I}} = 1k_{\mathrm{B}}T$, $u_{\mathrm{G}} = 1k_{\mathrm{B}}T$ and $u = 0.8u^{*}$. A comparison of snapshot sequences shown in figures 9(a) and (b) shows clearly that the monocentric pattern is formed faster and larger if lipid rafts are present in the membranes, which is qualitatively consistent with the recent experimental results reported in reference [37].

To assess the influence of lipid rafts on the temporal stability of the monocentric pattern, we next consider a situation when force f pushes TCRs toward the center of the contact zone for an initial time

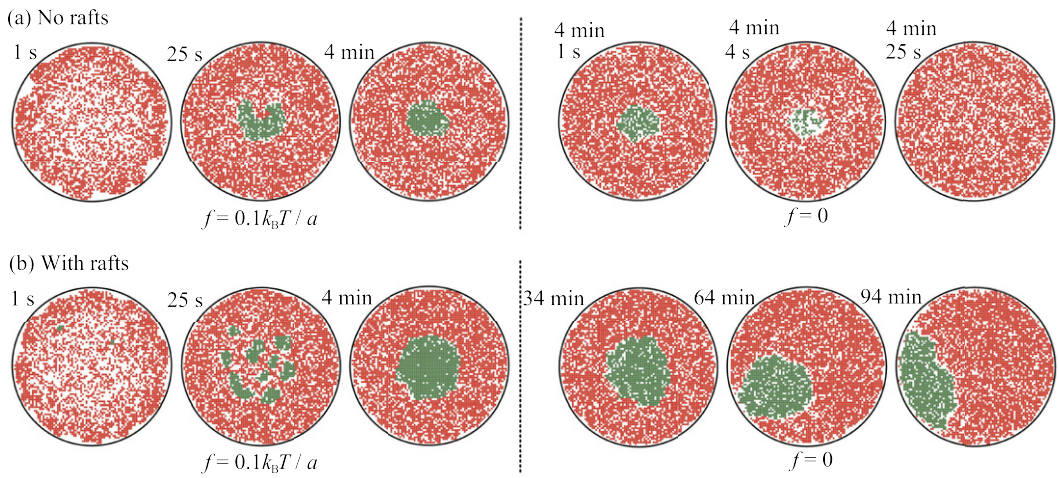

Figure 10. Typical pattern evolution during and after the active transport of TCRs to the center of the contact zone. Panels (a) and (b) correspond to the absence and presence of lipid rafts, respectively. In the MC simulations, force $f = 0.1k_BT/a$ acts concentrically on TCRs for the initial time interval of 4 min, after which the central supramolecular pattern is stable. Then the force is released, i.e., set to $f = 0$ in the MC simulations. The values of other parameters are identical as in the scenario shown in figure 9. Here, in the presence of lipid rafts (b), the monocentric pattern is larger and persists for a much longer time after the force is released.

interval t_f, after which the force is released, i.e. set to $f = 0$. Figure 10 shows two pattern sequences obtained from MC simulations with identical parameters as in the scenario shown in figure 9, except for the value of force f. Here, $f = 0.1k_BT/a$, which is an order of magnitude larger than in the scenario shown in figure 9. In both of the pattern sequences shown in figure 10, the monocentric pattern forms before $t_f = 4$ min. In the absence of lipid rafts (figure 10(a)), the TCR–MHCp complexes dissociate and the monocentric pattern vanishes within several minutes after the release of force f. In the presence of lipid rafts (figure 10(b)), however, the monocentric pattern persists for about 1 h. Therefore, the association of the TCR and MHCp molecules with lipid rafts significantly prolongs the lifetime of the intermediate monocentric pattern. Our simulation results here suggest that, in order to form the monocentric patterns for immune response, T cell might consume certain amount of ATP molecules to generate a relatively large force to pull TCRs in the initial stage of contact with APC. Later on, lipid rafts in the membranes help to stabilize the as-formed adhesion pattern and therefore less consumption of ATP is sufficient for T cell to maintain the compact structure of immunological synapse. It would be very interesting to test experimentally whether such a strategy is utilized by T cells.

In our simulations without active transport of TCRs, all the intermediate patterns eventually evolve into the structure with a lens-shape TCR–MHCp domain at the rim of the contact zone. This final pattern can be understood by considering the line tensions at the domain boundaries and at the rim of the contact zone, as explained in reference [45]. The line tension λ at TCR–MHCp and LFA1–ICAM domain boundaries is responsible for the phase separation and mainly caused by the curvature-mediated repulsion between the two type of complexes due to their length difference. The energy per length for forming a TCR–MHCp or LFA1–ICAM1 domain at the rim defines the line tension λ_{TM} or λ_{LI}, respectively. The difference $\lambda_{rim} = \lambda_{TM} - \lambda_{LI}$ then denotes the energy cost per length for replacing a TCR–MHCp domain at the rim by a LFA1–ICAM1 domain. Since the formation of a 15 nm-long TCR–MHCp complex imposes a larger reduction in the membrane separation at the rim than that of a 40 nm-long LFA1–ICAM1 complex, and the separation difference between 15 and 40 nm at the rim should not cause a large difference in the membrane elastic energy change, one would expect a small positive value for λ_{rim}. When λ is larger than λ_{rim}, boundaries of the TCR–MHCp domain inside the contact zone are energetically less favorable than boundaries at the rim, leading to the final lens-shape domain of TCR–MHCp at the rim of the contact zone. The final patterns shown in figures 2(b) and S3 obtained from simulations with different values of membrane separation l_{rim} at the contact zone rim seem to support the argument that λ is larger than λ_{rim}.

4. Conclusions

The onset and maintenance of adaptive immune responses depend sensitively on the spatial organization of interacting molecules at the interface between the T cell and the APC. Lipid rafts, which are dynamic microdomains in cell membranes, are implicated in the modulation of immune signaling by serving as

molecular sorting platforms. An important question is how lipid rafts affect the spatio-temporal patterns of adhesion molecules in the immunological synapse. To address this question, we used MC simulations of a statistical mesoscopic model with biologically relevant parameters. Our simulations give quantitative predictions on the influence of lipid rafts on the spatial distribution of the TCR–MHCp and LFA1–ICAM1 protein complexes during T-cell adhesion. At the time scale of several first seconds after the contact of the APC and T-cell membranes, lipid rafts can facilitate formation of clusters of TCR–MHCp complexes (figure 2). At intermediate time scales, i.e. between several minutes and about 1 h after the membrane contact, the TCR–MHCp clusters coalesce, grow and form one of the three possible patterns: (i) the monocentric pattern consisting of a central domain of TCR–MHCp complexes surrounded by a ring-shaped domain of LFA1–ICAM1 complexes, (ii) the inverted monocentric pattern consisting of a central domain of LFA1–ICAM1 complexes surrounded by a ring-shaped domain of TCR–MHCp complexes, or (iii) the multifocal pattern with several separate domains of TCR–MHCp complexes. We find that the intermediate patterns depend strongly on both the amount and physicochemical properties of lipid rafts (figures 2–8). Interestingly, association of the TCR–MHCp complexes with lipid rafts can lead to formation of the intermediate monocentric pattern even in the absence of active transport of the TCR molecules toward the center of the adhesion zone (figure 5). In addition, lipid rafts have a strong stabilizing effect on the monocentric pattern after its formation by the TCR active transport (figure 10). These findings not only supplement and extend the simulation results reported in references [45, 46, 48] but also help to explain the recent discovery that increased cholesterol levels in the T-cell membrane cause the immunological synapse to form faster and have a more compact structure [37].

Relevant control parameters in the process of membrane adhesion are the receptor–ligand interactions. In particular, the energy of binding of TCR and MHCp is affected by physicochemical properties of the peptide displayed on the MHC molecule. Our results quantify how changes in the TCR–MHCp binding energy, u_{TM}, affect the appearance of the intermediate patterns in the absence of the TCR active transport by the actin cytoskeleton (figure 5). Interestingly, if the adhering membranes contain lipid rafts (figure 5(b)), there can be a range of LFA1–ICAM1 binding energies, u_{LI}, in which the intermediate patterns (i), (ii) and (iii) are displayed in sequence as u_{TM} is increased. If the membranes bear no lipid rafts (figure 5(a)), however, only transitions between the intermediate patterns (i) and (ii) can be achieved by changing u_{TM} in the absence of the TCR active transport. Therefore, the physicochemical properties of the peptide on the MHC molecule seem to have a larger impact on the intermediate patterns of the TCR–MHCp complexes if the membranes contain lipid rafts.

Data availability statement

All data that support the findings of this study are included within the article (and any supplementary files).

Acknowledgments

L Li, J Hu and F Song acknowledge support from the NSFC Basic Science Center Program for ‘Multiscale Problems in Nonlinear Mechanics’ (11988102), the National Natural Science Foundation of China (Grant Nos. 21973040, 21504038, 11902327 and 11972041), the Strategic Priority Research Program of the Chinese Academy of Sciences (Grant No. XDB22040102), Youth Innovation Promotion Association CAS and Opening Fund of State Key Laboratory of Nonlinear Mechanics. J Hu also acknowledges support from the Fundamental Research Funds for the Central Universities (Grant No. 14380228) and the Shenzhen Science and Technology Innovation Committee (Grant Nos. JCYJ20200109150656717 and JCYJ20170818110613113). B Różycki acknowledges support from the National Science Center, Poland, Grant No. 2016/21/B/NZ1/00006. The simulations were performed on the computing facilities in the High Performance Computing Center (HPCC) of Nanjing University.

ORCID iDs

Jinglei Hu https://orcid.org/0000-0002-5758-2879
Bartosz Różycki https://orcid.org/0000-0001-5938-7308
Helong Wu https://orcid.org/0000-0002-7140-2184
Fan Song https://orcid.org/0000-0001-7359-2519

References

[1] Garcia K C, Degano M, Stanfield R L, Brunmark A, Jackson M R, Peterson P A, Teyton L and Wilson I A 1996 *Science* **274** 209–19
[2] van der Merwe P A, McNamee P N, Davies E A, Barclay A N and Davis S J 1995 *Curr. Biol.* **5** 74–84
[3] Wang J-H, Smolyar A, Tan K, Liu J-H, Kim M, Sun Z-Y, Wagner G and Reinherz E L 1999 *Cell* **97** 791–803
[4] Milstein O *et al* 2008 *J. Biol. Chem.* **283** 34414–22
[5] Dustin M L and Cooper J A 2000 *Nat. Immunol.* **1** 23–9
[6] Shaw A S and Dustin M L 1997 *Immunity* **6** 361–9
[7] Różycki B, Lipowsky R and Weikl T R 2010 *New J. Phys.* **12** 095003
[8] Krobath H, Różycki B, Lipowsky R and Weikl T R 2011 *PLoS One* **6** e23284
[9] Monks C R F, Freiberg B A, Kupfer H, Sciaky N and Kupfer A 1998 *Nature* **395** 82–6
[10] Krummel M F, Sjaastad M D, Wulfing C and Davis M M 2000 *Science* **289** 1349–52
[11] Potter T A, Grebe K, Freiberg B and Kupfer A 2001 *Proc. Natl Acad. Sci.* **98** 12624–9
[12] Grakoui A, Bromley S K, Sumen C, Davis M M, Shaw A S, Allen P M and Dustin M L 1999 *Science* **285** 221–7
[13] Johnson K G, Bromley S K, Dustin M L and Thomas M L 2000 *Proc. Natl Acad. Sci.* **97** 10138–43
[14] Lee K-H, Holdorf A D, Dustin M L, Chan A C, Allen P A and Shaw A S 2002 *Science* **295** 1539–42
[15] Hailman E, Burack W R, Shaw A S, Dustin M L and Allen P A 2002 *Immunity* **16** 839–48
[16] Richie L I, Ebert P J R, Wu L C, Krummel M F, Owen J J T and Davis M M 2002 *Immunity* **16** 595–606
[17] Qi S Y, Groves J T and Chakraborty A K 2001 *Proc. Natl Acad. Sci.* **98** 6548–53
[18] Weikl T R, Groves J T and Lipowsky R 2002 *Europhys. Lett.* **59** 916–22
[19] Burroughs N J and Wülfing C 2002 *Biophys. J.* **83** 1784–96
[20] Raychaudhuri S, Chakraborty A K and Kardar M 2003 *Phys. Rev. Lett.* **91** 208101
[21] Coombs D, Dembo M, Wofsy C and Goldstein B 2004 *Biophys. J.* **86** 1408–23
[22] Figge M T and Meyer-Hermann M 2006 *PLoS Comput. Biol.* **2** e171
[23] Wulfing C and Davis M M 1998 *Science* **282** 2266–9
[24] Choudhuri K and Dustin M L 2010 *FEBS Lett.* **584** 4823–31
[25] Lillemeier B F, Mörtelmaier M A, Forstner M B, Huppa J B, Groves J T and Davis M M 2010 *Nat. Immunol.* **11** 90–6
[26] Molnár E, Deswal S and Schamel W W A 2010 *FEBS Lett.* **584** 4832–7
[27] Springer T A 1990 *Nature* **346** 425–34
[28] Lingwood D and Simons K 2010 *Science* **327** 46–50
[29] Simons K and Sampaio J L 2011 *Cold Spring Harbor Perspect. Biol.* **3** a004697
[30] Levental I and Veatch S L 2016 *J. Mol. Biol.* **428** 4749–64
[31] Levental I, Levental K R and Heberle F A 2020 *Trends Cell Biolo.* **30** 341–53
[32] Li L, Hu J, Różycki B and Song F 2020 *Nano Lett.* **20** 722–8
[33] Stone M B, Shelby S A, Núñez M F, Wisser K and Veatch S L 2017 *eLife* **6** e19891
[34] Schamel W W, Arechaga I, Risueño R M, van Santen H M, Cabezas P, Risco C, Valpuesta J M and Alarcón B 2005 *J. Exp. Med.* **202** 493–503
[35] Zech T, Ejsing C S, Gaus K, de Wet B, Shevchenko A, Simons K and Harder T 2009 *EMBO J.* **28** 466–76
[36] Molnár E *et al* 2012 *J. Biol. Chem.* **287** 42664–74
[37] Yang W *et al* 2016 *Nature* **531** 651–5
[38] Newton R H *et al* 2018 *Nat. Immunol.* **19** 838–48
[39] Burack W R, Lee K-H, Holdorf A D, Dustin M L and Shaw A S 2002 *J. Immunol.* **169** 2837–41
[40] Dustin M L and Muller J 2016 *Science* **352** 516–7
[41] Janes P W, Ley S C, Magee A I and Kabouridis P S 2000 *Semin. Immunol.* **12** 23–34
[42] Simons K and Toomre D 2000 *Nat. Rev. Mol. Cell Biol.* **1** 31–9
[43] Anderson H A, Hiltbold E M and Roche P A 2000 *Nat. Immunol.* **1** 156–62
[44] Anderson H A and Roche P A 2015 *Biochim. Biophys. Acta Mol. Cell Res.* **1853** 775–80
[45] Weikl T R and Lipowsky R 2004 *Biophys. J.* **87** 3665–78
[46] Dharan N and Farago O 2017 *Soft Matter* **13** 6938–46
[47] Krobath H, Różycki B, Lipowsky R and Weikl T R 2009 *Soft Matter* **5** 3354–61
[48] Knezevic M, Jiang H D and Wang S S 2018 *Phys. Rev. Lett.* **121** 238101
[49] Simson R, Wallraff E, Faix J, Niewöhner J, Gerisch G and Sackmann E 1998 *Biophys. J.* **74** 514–22
[50] Carbone C B, Kern N, Fernandes R A, Hui E, Su X, Garcia K C and Vale R D 2017 *Proc. Natl Acad. Sci. USA.* **114** E9338–45
[51] Bush D R and Chattopadhyay A K 2014 *Phys. Rev.* E **90** 042706
[52] James J R and Vale R D 2012 *Nature* **487** 64–9
[53] Carlson A and Mahadevan L 2015 *PLoS Comput. Biol.* **11** e1004481
[54] Manz B N, Jackson B L, Petit R S, Dustin M L and Groves J 2011 *Proc. Natl Acad. Sci.* **108** 9089–94
[55] Pierce S K 2002 *Nat. Rev. Immunol.* **2** 96–105
[56] Pike L J 2009 *J. Lipid Res.* **50** S323–8
[57] Gupta N, Wollscheid B, Watts J D, Scheer B, Aebersold R and DeFranco A L 2006 *Nat. Immunol.* **7** 625–33
[58] Miceli M C, Moran M, Chung C D, Patel V P, Low T and Zinnanti W 2001 *Semin. Immunol.* **13** 115–28
[59] Marwali M R, MacLeod M A, Muzia D N and Takei F 2004 *J. Immunol.* **173** 2960–7
[60] Shamri R, Grabovsky V, Feigelson S W, Dwir O, Van Kooyk Y and Alon R 2002 *J. Biol. Chem.* **277** 40027–35
[61] Hegde V L, Singh N P, Nagarkatti P S and Nagarkatti M 2008 *J. Leukocyte Biol.* **84** 134–42
[62] Shao B *et al* 2015 *Proc. Natl Acad. Sci. USA.* **112** 8661–6
[63] DeMond A L, Mossman K D, Starr T, Dustin M L and Groves J T 2008 *Biophys. J.* **94** 3286–92
[64] Li L, Hu J, Shi X, Shao Y and Song F 2017 *Soft Matter* **13** 4294–304
[65] Ramadurai S, Holt A, Krasnikov V, van den Bogaart G, Killian J A and Poolman B 2009 *J. Am. Chem. Soc.* **131** 12650–6
[66] Gambin Y, Lopez-Esparza R, Reffay M, Sierecki E, Gov N S, Genest M, Hodges R S and Urbach W 2006 *Proc. Natl Acad. Sci.* **103** 2098–102